Optimizing Power Generation of a Bottom-Raised Oscillating Surge Wave Energy Converter using a Theoretical Model

Preprint

Nhu Nguyen,[1] Jacob Davis,[1] Krish Thiagarajan,[1]
Nathan Tom,[2] and Cole Burge[3]

1 University of Massachusetts Amherst
2 National Renewable Energy Laboratory
3 University of Washington

Presented at the 14th European Wave and Tidal Energy Conference
Plymouth, United Kingdom
September 5–9, 2021

NREL is a national laboratory of the U.S. Department of Energy
Office of Energy Efficiency & Renewable Energy
Operated by the Alliance for Sustainable Energy, LLC

This report is available at no cost from the National Renewable Energy Laboratory (NREL) at www.nrel.gov/publications.

Contract No. DE-AC36-08GO28308

Conference Paper
NREL/CP-5700-79929
October 2021

Optimizing Power Generation of a Bottom-Raised Oscillating Surge Wave Energy Converter using a Theoretical Model

Preprint

Nhu Nguyen,[1] Jacob Davis,[1] Krish Thiagarajan,[1]
Nathan Tom,[2] and Cole Burge[3]

1 University of Massachusetts Amherst
2 National Renewable Energy Laboratory
3 University of Washington

Suggested Citation
Nguyen, Nhu, Jacob Davis, Krish Thiagarajan, Nathan Tom, and Cole Burge. 2021. *Optimizing Power Generation of a Bottom-Raised Oscillating Surge Wave Energy Converter using a Theoretical Model: Preprint*. Golden, CO: National Renewable Energy Laboratory. NREL/CP-5700-79929. https://www.nrel.gov/docs/fy22osti/79929.pdf.

NREL is a national laboratory of the U.S. Department of Energy
Office of Energy Efficiency & Renewable Energy
Operated by the Alliance for Sustainable Energy, LLC

This report is available at no cost from the National Renewable Energy Laboratory (NREL) at www.nrel.gov/publications.

Contract No. DE-AC36-08GO28308

Conference Paper
NREL/CP-5700-79929
October 2021

National Renewable Energy Laboratory
15013 Denver West Parkway
Golden, CO 80401
303-275-3000 • www.nrel.gov

NOTICE

This work was authored in part by the National Renewable Energy Laboratory, operated by Alliance for Sustainable Energy, LLC, for the U.S. Department of Energy (DOE) under Contract No. DE-AC36-08GO28308. Funding provided by the U.S. Department of Energy Office of Energy Efficiency and Renewable Energy Water Power Technologies Office. The views expressed herein do not necessarily represent the views of the DOE or the U.S. Government. The U.S. Government retains and the publisher, by accepting the article for publication, acknowledges that the U.S. Government retains a nonexclusive, paid-up, irrevocable, worldwide license to publish or reproduce the published form of this work, or allow others to do so, for U.S. Government purposes.

Cover Photos by Dennis Schroeder: (clockwise, left to right) NREL 51934, NREL 45897, NREL 42160, NREL 45891, NREL 48097, NREL 46526.

Optimizing power generation of a bottom-raised oscillating surge wave energy converter using a theoretical model

Nhu Nguyen, Jacob Davis, Krish Thiagarajan, Nathan Tom, and Cole Burge

Abstract—**Preliminary sizing of an oscillating surge wave energy converter (OSWEC) is an iterative process that relies on knowledge of the relevant hydrodynamic coefficients for a given geometry. Often, the complex definition of the device geometry requires coefficients to be obtained through experiments or numerical boundary element solvers such as WAMIT. These techniques demand significant user and computational effort, therefore inhibiting the fine-scale parametrization of object dimensions. In this study, a theoretical model, originally presented in Michele et al. (2016), is developed and demonstrated to efficiently optimize the power production for an OSWEC device (subjected to certain environmental conditions) with variations in device widths, heights, and distances from the seabed. Assuming negligible device thickness, the OSWEC motions are modeled as a bottom-raised two-dimensional flap in regular waves using potential flow theory formulated in elliptical coordinates. The solutions to this diffraction-radiation problem are obtained using Mathieu functions with appropriate boundary conditions. The resulting potentials are then used to derive frequency-dependent expressions for the added mass and radiation-damping coefficients, along with wave-excitation magnitude in surge, pitch, and coupled surge-pitch motions. Good agreement in hydrodynamic coefficient curves is shown between the theoretical model and the numerical results obtained from the boundary element-based program WAMIT. The theoretical model is then employed to maximize the time-averaged output power while maintaining or reducing the hinge reaction force, with variations in device dimensions, wave frequency, and amplitude.**

Keywords—**OSWEC, hydrodynamic coefficients, added moment of inertia, wave radiation damping, wave excitation, wave energy converter, power production, ACE.**

I. Introduction

From design space exploration to detailed design, wave energy converter (WEC) developers employ a range of tools to optimize performance. Multiple optimization frameworks are available to designers for characterizing and refining the performance of OSWEC devices [1][2]. Typically, these require analyses using analytical, semi-numerical, or numerical methods. Among these approaches, theoretical (analytical-based) models benefit from their simple setup and quick computational time. These methods, however, tend to be limited to simple geometries (i.e., geometries in which fine-scale details are not present or are neglected [3][4]). Hence, these approaches are well-suited for early stages of development, including design space exploration and the optimization of device geometry.

The current study presents a theoretical optimization framework for the development of bottom-fixed, oscillating surge wave energy converters (OSWECs), first introduced by Michele et al. in [3], and expands it to model bottom-raised devices. A particular emphasis is placed on optimization for structural and power production performance, though such a framework could readily be extended to additional performance metrics.

The authors in [3] proposed to characterize the body's hydrodynamics by solving the radiation and scattering potentials using the angular and radial Mathieu functions. The potential flow problem is transformed into an elliptical coordinate system in which the body of the flap is represented by the ellipse at $\xi = 0$ (lying over the traditional x-axis) thereby allowing the problem to be

ID number: 2202

Nhu Nguyen is with the Mechanical Engineering Department at University of Massachusetts Amherst, Amherst, Massachusetts, USA (email: Nvnguyen@umass.edu). Please address all correspondence to this author.

Jacob R. Davis is with the Mechanical Engineering Department at University of Massachusetts Amherst, Amherst, Massachusetts, USA (email: Jacrdavis@umass.edu).

Krish Thiagarajan (full name: Krish Thiagarajan Sharman) is with the Mechanical Engineering Department at University of Massachusetts Amherst, Amherst, Massachusetts, USA (email: Kthiagarajan@umass.edu).

Nathan Tom is with the National Renewable Energy Laboratory, Golden, Colorado, USA (email: Nathan.Tom@nrel.gov).

Cole Burge is with the University of Washington, Seattle, Washington, USA (email: coleburge@gmail.com).

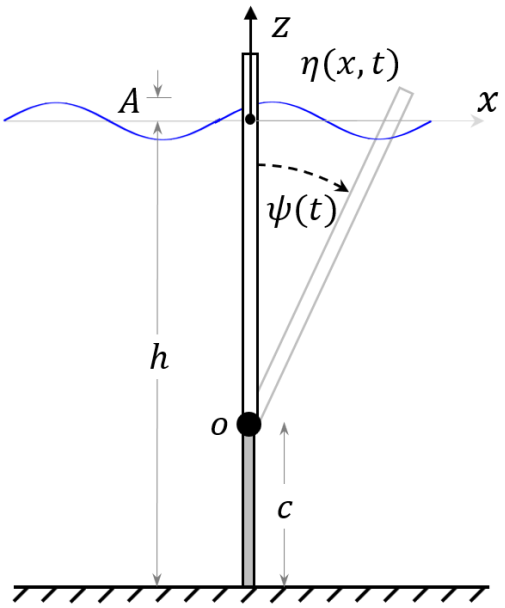

Fig. 1. Definition of the OSWEC system in Cartesian coordinates.

solved. In this representation, the body thickness must be equated to zero.

For semi-numerical techniques, Renzi and Dias's series of papers have proposed using Green's integral theorem along with a hypersingular integral in potential flow equation to predict the hydrodynamics of a single OSWEC with negligible thickness [5]–[7]. The method has been applied to study the OSWEC performances in both open ocean and in a channel. Michele *et al.* [8] later extended the integral approach to study the motions of an array of devices with finite thickness. Employing a different approach, Noad and Porter introduced Fourier transforms and Galerkin expansion methods to study the behaviors of both the surface piercing and the fully submerged OSWECs [4].

Compared to the aforementioned techniques, numerical methods are generally not limited to certain geometric features and thus often employed more widely in the research of WEC system motions. Within this approach, boundary element method (BEM) is considered as one of the most popular due to its relatively faster computational speed compared to other methods using a computational fluid dynamics (CFD) technique. Several studies have employed this technique to successfully investigate the performance of the OSWEC including [1][9]. Similar to the semi-numerical technique, numerical modeling also requires significant user, programming, and computational efforts, which could inhibit the fine-scale parametrization of objective dimensions.

The initial sizing of a WEC is an iterative process which relies on knowledge of the relevant hydrodynamic coefficients for a wide range of geometric parameters. Due to this reason, the analytical model can be seen as the most effective and least time-consuming approach for this purpose. In this paper, a theoretical model extending the works originally introduced in [3] is developed to predict the hydrodynamic coefficients of a bottom-raised OSWEC (Fig. 1). An analytical model for the coupling surge-pitch coefficients along with the wave-excitation load are also derived. The formulas are employed to efficiently optimize the power production for an OSWEC device subjected to certain environmental conditions. Device performances subjected to variations in widths, heights, and distances from the seabed are investigated. Power production along with the ACE matrix are also evaluated. Comparisons with numerical results and computational speed from WAMIT are also discussed.

II. Mathematical Formulae

A. *Analytical model for hydrodynamic coefficients*

This study builds upon the analytical solutions described in Michele *et al.* [3], which models the motion of an array of flap gates or bottom-fixed OSWECs employing a thin plate assumption in an elliptical coordinate system. It is noted that while the following analysis can be extended to an array of devices similar to Michele's study, the current work focuses on demonstrating the power optimization of one OSWEC system. The current work also extends previous research to account for bottom-raised foundations. Surge-pitch hydrodynamic coefficients, which are used to evaluate structural loadings on the foundation, are also formulated.

In order to employ the thin plate assumption, the thickness of the device is considered negligible compared to its width. For a point (x, y, z) in the incompressible and irrotational fluid domain, there exists a velocity potential, $\mathbf{\Phi}(x, y, z, t)$ that satisfies the Laplace's equation such that:

$$\nabla^2 \mathbf{\Phi}(x, y, z, t) = 0 \tag{1}$$

We assume that the flap undergoes regular harmonic motion with frequency ω around the y-axis (Fig. 1) as

$$\psi(t) = Re\{\Psi e^{-i\omega t}\} \tag{2}$$

Here, Ψ is the complex amplitude of rotation. The temporal component in the velocity potential can be separated out (or rewritten) as

$$\mathbf{\Phi}(x, y, z, t) = Re\{\phi(x, y, z) e^{-i\omega t}\} \tag{3}$$

On the other hand, the spatial potential can be written as a linear combination of incident wave potential (ϕ^I), scattered wave potential (ϕ^S) induced by the presence of the OSWEC, and the radiated wave potential (ϕ^R) due to the motions of the flap.

$$\phi(x, y, z) = \phi^I + \phi^S + \phi^R \tag{4}$$

With

$$\phi^I = -\frac{iAg}{\omega} \frac{\cos h\, k_o(h + z)}{\cosh k_o h} e^{-ik_o(x\cos\theta + y\sin\theta)} \tag{5}$$

Here, A and k_o are the wave amplitude and wave number, whose values are derived from the roots of the dispersion relation $\omega^2 = g k_o \tanh k_o h$. $g = 9.81\ \mathrm{m/s^2}$ and i denote the gravitational constant and the imaginary unit, respectively. θ represents the relative angle of the incident

wave with respect to the x-axis, and h is the water depth. It is noted that both ϕ^S and ϕ^R should satisfy Laplace's equation.

In order to obtain the solutions to Eq. (1), the following boundary conditions are applied to the problem:

1. Mixed (dynamic + kinematic) boundary condition at the free surface ($z = 0$):

$$\mathbf{\Phi}_{\mathrm{tt}} + \mathrm{g}\mathbf{\Phi}_{\mathrm{z}} = 0 \tag{6}$$

2. No flux condition on the sea bottom ($z = -h$):

$$\mathbf{\Phi}_{\mathrm{z}} = 0 \tag{7}$$

3. Kinematic condition (no through flow) on the flap's surfaces $z \in [-h, 0]$):

$$\begin{aligned}\mathbf{\Phi}_{\mathrm{x}} &= -\psi_t * (z + h - c) * H(z + h - c) \\ &= i\omega\Psi * (z + h - c)e^{-i\omega t} \\ &* H(z + h - c)\end{aligned} \tag{8}$$

4. ϕ^S and ϕ^R must be bounded as $\sqrt{x^2 + y^2} \to \infty$ (9)

Here, subscripts denote derivatives (with respect to the corresponding variables) H is the Heaviside step function, and c denotes the distance from the seafloor to the hinge of the OSWEC. The third condition (Eq. (7)) is established from the rotational motion of the flap in Cartesian coordinates. The flap strictly rotates around the y-axis (Fig. 1) such that its motion is in the x-z plane. Assuming small-amplitude oscillation, the horizontal velocities, $\mathbf{\Phi}_{\mathrm{x}}$, of the flap's surface (and the fluid particles next to the flap) are calculated using the rate of rotation, ψ_t, times the distance from the hinge.

The solutions to the boundary value problems described above are only possible through semi-analytical and numerical methods. To seek a full analytical solution, Michele and coauthors proposed transforming the problem to elliptical coordinates (ξ, η, z), whose values are defined as

$$x = \frac{w}{2}\sinh\xi\sin\eta \quad , \quad y = \frac{w}{2}\cosh\xi\cos\eta \quad , \quad z = z \tag{10}$$

Here, w represents the width of the OSWEC device. The conversion benefits from the thin plate assumption, due to the fact that with $\xi = 0$, the ellipse collapses into a segment of width w representing the OSWEC flap. All the points on the flap's surfaces can be described by $\xi = 0$ and $\eta \in [0, 2\pi]$. This simplification makes it possible to formulate ϕ^R, ϕ^S, and subsequently the hydrodynamic coefficients of added inertia, μ, and radiation damping, ν.

The expressions of ϕ^R and ϕ^S in Eq. (4) can be written as

$$\begin{cases}\phi^R = \varphi_n^R(x, y)Z(z) \\ \phi^S = \varphi_n^S(x, y)Z(z)\end{cases} \tag{11}$$

From separation of variables and using the conditions that both ϕ^R and ϕ^S satisfy the Laplace's equation, the following equation is obtained:

$$Z'' - k^2 Z = 0 \tag{12}$$

Employing boundary conditions at the sea bottom (7) and on the water surface (6), the dispersion relation can be derived and the value of k is evaluated as the root of

$$\omega^2 = gk\tanh(kh) \tag{13}$$

For imaginary eigenvalue $k = i\kappa$, κ corresponds to the real solutions of

$$\omega^2 = -g\kappa_n\tan(\kappa_n h) \quad , \quad n = 1,2,3 \ldots \tag{14}$$

It is noted that there is an infinite number of roots to the equation above. With the solutions of k_n, the corresponding normalized eigenfunction is derived as (see [10] for more details)

$$Z_n(z) = \frac{\sqrt{2}\cosh k_n(h + z)}{\left(h + \left(\frac{g}{\omega^2}\right)\sinh^2 k_n h\right)^{\frac{1}{2}}} \quad , \quad \mathrm{n} = 0,1,2,3 \ldots \tag{15}$$

On the other hand, converting the Laplace's equations for $\varphi^R(x, y)$ and $\varphi^S(x, y)$ to the elliptical system, the two-dimensional Helmholtz equations can be obtained

$$\left[\frac{\partial^2}{\partial\xi^2} + \frac{\partial^2}{\partial\eta^2} + \frac{w^2k_n^2}{8}(\cosh 2\xi - \cos 2\eta)\right]\begin{Bmatrix}\varphi^R(\xi, \eta) \\ \varphi^S(\xi, \eta)\end{Bmatrix} = 0 \tag{16}$$

The general solutions to the Helmholtz equation in these coordinates are obtained using the solutions of the angular Mathieu and Hankel-Mathieu equations. These are analogous to the use of trigonometric functions in the Cartesian system or Bessel functions in cylindrical coordinates. Applying the boundary conditions specified in (6)-(9), the solutions of the radiated potential are derived as [3]

$$\begin{aligned}\varphi_n^R(\xi, \eta) = \; & -i\omega\Psi\mathrm{f_n}w * \\ & \sum_{m=0}^{\infty}\frac{B_1^{(2m+1)}Ho_{2m+1}^{(1)}(\xi = 0, \tau_n)se_{2m+1}(\eta, \tau_n)}{2Ho_{\xi\,2m+1}^{(1)}(0, \tau_n)}\end{aligned} \tag{17}$$

With

$$f_n = \frac{\sqrt{2}[k_n(h - c)\sinh k_n h + \cosh k_n c - \cosh k_n h]}{k_n^2(h + (g/\omega^2)\sinh^2 k_n h)^{\frac{1}{2}}} \tag{18}$$

Here, $Ho^{(1)}$ and se are called the odd Hankel-Mathieu and Mathieu functions of the first kind with order m, respectively. Ho_ξ is the derivative of Ho with respect to ξ. B_1 refers to the first coefficient associated with se functions (refer to [11] for more details on Mathieu functions). J_j is the Bessel function of the first kind and order j.

It is noted that the equations presented here are slightly different from those in [3], which were derived for a bottom-fixed OSWEC instead of bottom-raised system. The effect of the bottom-to-hinge distance, c, on the hydrodynamic characteristics, has been added. The changes are reflected in the expressions for f_n shown in (18). When $c = 0$, the f_n equation converges to that derived in [1].

The pitch-pitch hydrodynamic added inertia μ_{55}, radiation damping ν_{55}, and the wave-exciting torque X_5 are also obtained (from the normal surface integral of the velocity potential derivative) as

$$\mu_{55} = \rho w^2 \pi \sum_{n=0}^{\infty} f_n^2 \, Im\left\{\sum_{m=0}^{\infty} \frac{B_1^{(2m+1)^2} No_{2m+1}(0,\tau)}{4Ho_{\xi}^{(1)}{}_{2m+1}(0,\tau)}\right\} \quad (19)$$

$$\nu_{55} = -\rho\omega w^2 f_o^2 \pi \, Re\left\{\sum_{m=0}^{\infty} \frac{B_1^{(2m+1)^2} No_{2m+1}(0,\tau)}{4Ho_{\xi}^{(1)}{}_{2m+1}(0,\tau)}\right\} \quad (20)$$

And

$$X_5 = \rho\omega A w^2 f_o d_o \pi \cos\theta \left\{\sum_{m=0}^{\infty} \frac{B_1^{(2m+1)^2} No_{2m+1}(0,\tau)}{4Ho_{\xi}^{(1)}{}_{2m+1}(0,\tau)}\right\} \quad (21)$$

with

$$d_o = \frac{g k_o (h + (g/\omega^2)\sinh^2 k_o h)^{\frac{1}{2}}}{\sqrt{2}\omega \cosh k_o h} \quad (22)$$

Here, ρ is the fluid density. In order to quantify the structural performance characteristics of the OSWEC (discussed in the next section), the study also expands upon the work presented in [3] to derive the analytical formula for the surge wave load as

$$\begin{aligned} X_1 &= i\omega\rho \iint_{S_{body}} \phi^S(\xi,\eta,z) n_1 dS \\ &= -i\omega\rho \frac{w}{2} \iint_{S_{body}} \phi^S(\xi,\eta) Z_o(z) \sin\eta \, dz d\eta \end{aligned} \quad (23)$$

$$X_1 = \rho\omega A w^2 \lambda_o d_o \pi \cos\theta \left\{\sum_{m=0}^{\infty} \frac{B_1^{(2m+1)^2} No_{2m+1}(0,\tau)}{4Ho_{\xi}^{(1)}{}_{2m+1}(0,\tau)}\right\} \quad (24)$$

With

$$\lambda_n = \frac{\sqrt{2}(\sinh k_n h - sinh\, k_n c)}{k_n \left(h + \frac{g}{\omega^2}\sinh^2 k_n h\right)^{\frac{1}{2}}} \quad , \quad n = 0,1,2,3,\ldots \quad (25)$$

The hydrodynamic coefficients of surge-pitch added inertia, μ_{15}, and radiation damping, ν_{15}, are required to obtain the hinge surge reaction force and are derived as

$$\begin{aligned} \mu_{15} &= \frac{\rho}{\omega} \sum_{n=0}^{\infty} Im\left(\iint_{S_{body}} \phi_n^R(\xi,\eta) Z_n(z) n_1 dS\right) \\ &= \frac{\rho}{\omega}\frac{w}{2} \sum_{n=0}^{\infty} Im\left(\iint_{S_{body}} \phi_n^R(\xi,\eta) Z_n(z) \sin\eta \, dz \, d\eta\right) \end{aligned} \quad (26)$$

$$\mu_{15} = \rho w^2 \pi \sum_{n=0}^{\infty} f_n \lambda_n \, Im\left\{\sum_{m=0}^{\infty} \frac{B_1^{(2m+1)^2} No_{2m+1}(0,\tau)}{4Ho_{\xi}^{(1)}{}_{2m+1}(0,\tau)}\right\} \quad (27)$$

$$\begin{aligned} \nu_{15} &= -\rho Re\left(\iint_{S_{body}} \phi_o^R(\xi,\eta) Z_o(z) n_1 dS\right) \\ &= -\rho Re\left(\iint_{S_{body}} \phi_o^R(\xi,\eta) \frac{w}{2} \sin\eta \, d\eta \, Z_o(z) dz\right) \end{aligned} \quad (28)$$

$$\nu_{15} = -\rho\omega w^2 f_o \lambda_o \pi \, Re\left\{\sum_{m=0}^{\infty} \frac{B_1^{(2m+1)^2} No_{2m+1}(0,\tau)}{4Ho_{\xi}^{(1)}{}_{2m+1}(0,\tau)}\right\} \quad (29)$$

Lastly, the complex amplitude of pitch rotation relates to the frequency domain coefficients as

$$\Psi = \frac{AX_5}{-\omega^2(I_{55} + \mu_{55}) + i\omega(\nu_{55} + \nu_g) + C_{55} + C_g} \quad (30)$$

Where ν_g and C_g are the power take off (PTO) damping and restoring coefficients, respectively (to be discussed in the next section), I_{55} is the mass moment of inertia of a bottom-hinged flap, and C_{55} is the combined hydrostatic and gravitational restoring coefficient which derives from the first order truncation of the Taylor series expansion of the equation of motion [12]. The latter two are calculated as

$$I_{55} = \frac{1}{3} M H_f^2 \left(1 + \left(\frac{p}{2H_f}\right)^2\right) \quad (31)$$

$$C_{55} = (\rho \forall r_b - M r_g) g \quad (32)$$

Where M, H_f, and p are the mass, height, and thickness of the flap, $\forall$ is the displacement of the flap (here the entire body is submerged such that $\forall = wpH_f$), r_b is the center of buoyancy, and r_g is the center of gravity. These parameters will be defined for the validation and demonstration models in later sections.

B. Performance characterization

The early stages of sizing and design for a wave energy converter concept are often based on fundamental performance estimates—namely from metrics associated with power generation, capital costs, and structural considerations, among others. OSWEC designs, in particular, are largely driven by structural costs and limits resulting from the large hydrodynamic loads experienced during operation [6]. To demonstrate the utility of analytical modelling during the early stages of design, a few relevant performance characteristic metrics are defined here and used later to demonstrate a parametric study on the geometry of an OSWEC. Fortunately, many of the common, first-order metrics used in WEC design are readily calculated by the frequency domain hydrodynamic coefficients output by the model.

A common measure of wave energy converter power performance is the capture width (CW), defined as

$$CW = \frac{P_T}{wP_W} \quad (33)$$

Where P_T is the time-averaged power absorbed by the power take off (as defined in subsection *C, Power estimation*), w is the device width, and P_W is the time-averaged wave power per unit crest-width

$$P_W = \frac{1}{4}\rho g A^2 \sqrt{\frac{g}{k_o}\tanh k_o h}\left(1 + \frac{2k_o h}{\sinh 2k_o h}\right) \quad (34)$$

C. Power estimation

Power estimates are calculated assuming the power take-off is capable of providing variable damping to the system, controlled on a per-wave period basis. Under this

condition, the time-averaged power, per wave-amplitude squared, absorbed by an ideal PTO unit is [13]

$$\frac{P_T}{\mathrm{A}^2} = \frac{1}{4}\frac{|X_5|^2}{\nu_{55}}\frac{1}{1+\varepsilon} \tag{35}$$

Where the coefficient ε is defined as,

$$\varepsilon = \sqrt{1 + \left(\frac{C_{55} - \omega^2(I_{55} + \mu_{55})}{\omega \nu_{55}}\right)^2} \tag{36}$$

The optimal PTO damping coefficient is then related to the wave radiation damping by,

$$\nu_g = \nu_{55}\varepsilon \tag{37}$$

Provided the relevant hydrodynamic coefficients are available, the time-averaged power expression (35) can be computed as a function of wave frequency. With a known wave amplitude, the expression can be scaled to obtain an estimate of the capture width (33) for a given OSWEC geometry.

Rather than a single wave amplitude-frequency combination, some frequency domain metrics can be evaluated for an irregular sea state. For instance, a wave energy spectrum can readily be incorporated into the time-averaged power expression (35) to obtain statistics on the power production during an irregular sea state [14]. In its most basic form, the energy spectrum is a superposition of the energy components of each wave that contributes to an irregular sea state. The following relationship can be defined between the energy spectrum and each wave amplitude:

$$S(\omega)d\omega = \frac{1}{2}A_i^2 \tag{38}$$

Where $S(\omega)$ is the wave energy spectrum and A_i is the amplitude of each individual wave that contributes to the irregular sea state. This expression can be used in conjunction with the time-averaged power per wave-amplitude squared (35) and integrated over a range of frequencies to obtain the time-averaged power absorbed by the PTO:

$$P_T = \frac{1}{2}\int \frac{|X_5|}{\nu_{55}}\frac{1}{1+\varepsilon}S(\omega)d\omega \tag{39}$$

In this paper, the Bretschneider Spectrum is elected for use,

$$S(\omega) = \frac{5}{16}\frac{\omega_m^4}{\omega^5}H_{1/3}^2 \exp\left(-\frac{5}{4}\frac{\omega_m^4}{\omega^4}\right) \tag{40}$$

Where ω_m is the modal (or peak) frequency and $H_{1/3}$ is the significant wave height.

D. Structural Loads

Knowledge of the coupled surge-pitch added mass and damping coefficients derived in (27) and (29), respectively, enables the estimation of reaction forces at the hinge of the OSWEC (point *O* in Fig. 1). Centrifugal forces and force components in the heave direction are neglected in this exercise.

The hinge surge reaction force is [12]:

$$F_{R1} = (-\omega^2\mu_{15} + i\omega\nu_{15})\Psi - AX_1 \tag{41}$$

The contribution of this force to the bending moment at the base is then obtained as

$$M_b^o = c\,F_{R1} \tag{42}$$

With the substitution of (30) into (40), it is possible to obtain a spectrum of F_{R1} and thus M_b^o, from which further statistics can be extracted. Here, the hinge surge reaction force and base bending moment will instead be evaluated using the design wave concept, in which the spectrum is replaced with a single wave at the significant wave height and peak period (described in Section *IV. Demonstration*).

III. VALIDATIONS

E. Hydrodynamic coefficients and wave-exciting forces

To substantiate the proposed theoretical model, analytically obtained hydrodynamic coefficients are compared here with numerical results from WAMIT (version 7.2). The WAMIT model is representative of a laboratory-scale, bottom-raised OSWEC previously tested in a 4.5-m deep wave basin at the University of Maine's Harold Alfond W² Ocean Engineering Laboratory. Time-domain numerical simulations, produced using hydrodynamic coefficients from the WAMIT model, were previously validated against data from the wave basin experiments. The simulated and experimental time series trends compared exceptionally well, indicating the model hydrodynamic coefficients provide a valid representation of the real-world OSWEC dynamics. The dimensions and geometric properties of the system are detailed in Table 1. While the analytically obtained hydrodynamics are based on a thin-flap assumption, a finite thickness is defined to achieve an accurate mass moment of inertia.

TABLE 1
DIMENSIONS AND PROPERTIES OF THE VALIDATION MODEL

Symbol	Name	Value	Unit
h	Water depth	4.5	m
c	Hinge to seabed	3.85	m
H_f	Flap height	0.61	m
w	Flap width	0.94	m
p	Flap thickness	0.1	m
M	Flap mass	25.7	kg
I_{55}	Mom. inertia[a]	4.25	kg-m²
C_{55}	Linear hydrostatic restoring coeff.[a]	137	kg-m² s⁻²

[a] Calculated about the hinge point

Fig. 2 presents a comparison of the theoretical quantities derived in (19)—(29) with numerically obtained WAMIT quantities. These include the pitch added mass and radiation damping, surge-pitch added mass and radiation damping, pitch excitation moment magnitude and phase, and surge excitation moment magnitude and phase. Coefficients and excitation forces are evaluated over a

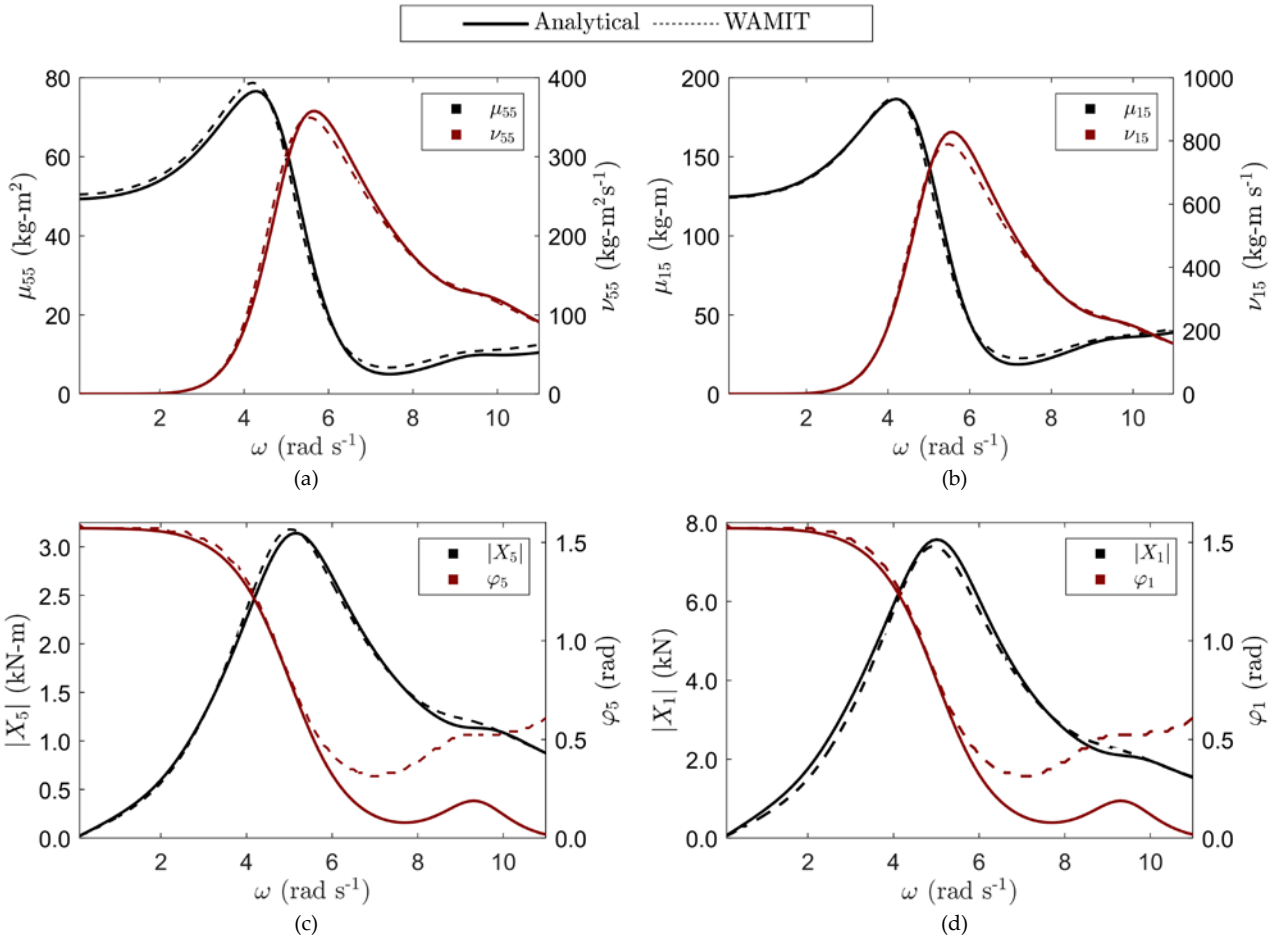

Fig. 2. Comparison of relevant hydrodynamic coefficients obtained using the analytical model (solid) and WAMIT (dashed). (a) pitch added mass and pitch wave radiation damping; (b) coupled surge-pitch added mass and coupled surge-pitch wave radiation damping; (c) wave-excitation pitch moment magnitude and phase; and (d) wave-excitation surge force magnitude and phase. All curves shown in black correspond to the left-hand axis, and curves shown in red correspond to the right-hand axis. All coefficients are calculated with respect to rotation about the flap hinge.

frequency range of 0.1 rad/s to 11 rad/s with a step size of 0.1 rad/s. A total of 15 frequencies ($n = 15$) were retained in the solution to (17).

Hydrodynamic results demonstrate good similarity between the numerical and theoretical calculations. The trends of the added mass, radiation damping, and wave excitation magnitude coefficients are captured well by the theoretical model. A notable deviation in the wave-excitation torque and force phase angles (subfigs c and d) is observed at higher frequencies; the analytical model predicts a convergence of the phase angles toward zero as the frequency increases, whereas the WAMIT model predicts an offset close to 30 degrees. These disparities begin at a frequency of 5 rad/s. Variations in the device thickness between the two models may be a key factor. The analytical model assumes a flat plate (negligible thickness), whereas the numerical model is representative of the physical model tested in the wave basin which has a width to thickness aspect ratio of 9.4. Differences in boundary conditions beneath the OSWEC may also contribute to deviation between the analytical and numerical results. The no-slip condition from $z \in [-h, c)$ in Eq. (8) is representative of a foundation that blocks flow beneath the OSWEC. This foundation is not modeled in WAMIT, which in turn enables nonzero flow velocities to be modeled beneath the device. The reason for this variation will be further investigated in a subsequent study.

Despite the small variations, the theoretical model shows clear advantage compared to the numerical calculations in computational speed. While the theoretical model takes only a few seconds to compute all the cases, it takes several minutes on average to run one frequency case in WAMIT.

IV. Demonstration

A great benefit of the use of theoretical models in WEC design derives from their ability to explore the available design space with computational ease. This capability is demonstrated here using the theoretical model to perform a sweep over a range of dimensions. Frequency-dependent performance metrics, defined in sections *C-D*, are evaluated as a function of parameterized OSWEC

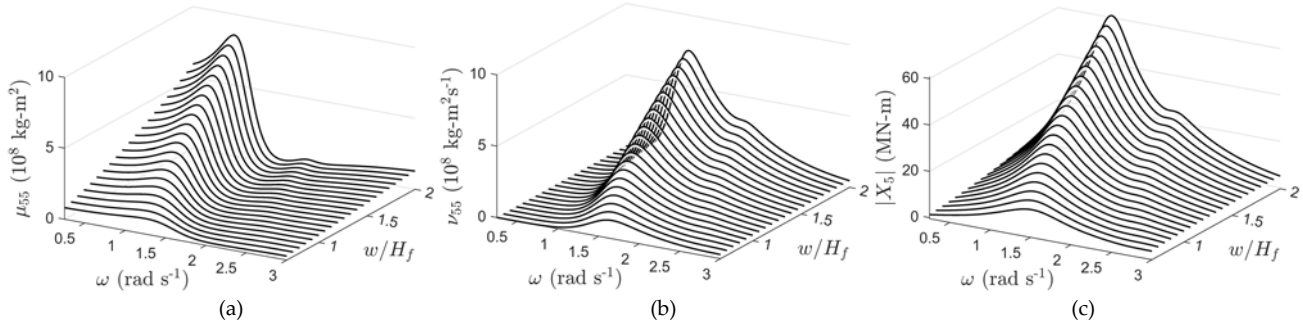

(a) (b) (c)

Fig. 3. Hydrodynamic coefficients as a function of frequency and normalized width w/H_f for a constant flap height $H_f = h/2$: (a) pitch added mass; (b) pitch radiation damping; (c) excitation pitch moment.

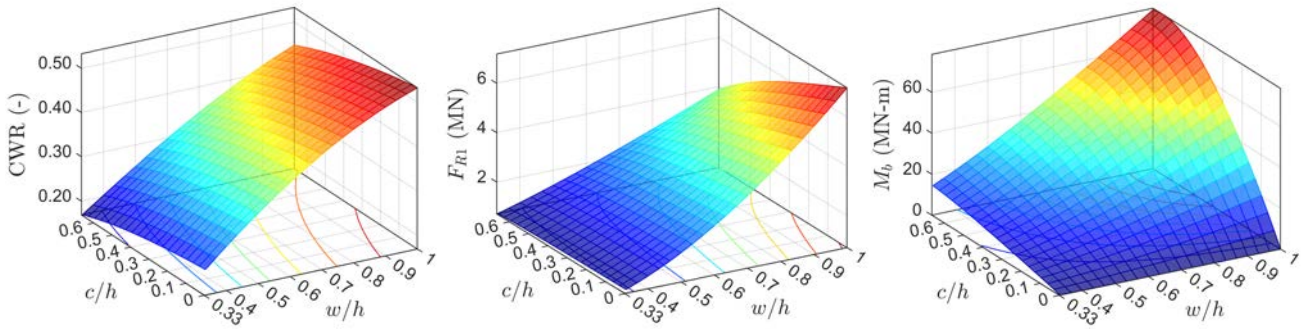

(a) (b) (c)

Fig. 4. Performance characterization metrics as a function of normalized distanced to seabed c/h and normalized width w/h: (a) capture width ratio; (b) surge hinge reaction force; (c) foundation base bending moment.

dimensions for a given set of environmental conditions. The environmental conditions, body dimensions, and demonstration results are discussed in the next sections.

F. *Environmental Conditions*

A full-scale irregular wave state from the U.S. Department of Energy Wave Energy Prize [16] was used to define the environmental wave conditions of the demonstration. Full-scale irregular wave state 2 (IWS 2) was elected for use. This wave state has a peak period $T_p = 9.86$ s significant wave height $H_s = 2.64$ m, and incident wave angle $\theta = 0$ deg. The irregular sea state was defined by a Bretschneider wave energy spectrum (38). The environmental conditions used in demonstration are summarized in Table 2.

TABLE 2
ENVIRONMENTAL CONDITIONS USED IN THE DEMONSTRATION

Symbol	Name	Value	Unit
$S(\omega)$	Energy spectrum	Bretschneider	-
T_p	Peak period	9.86	s
H_s	Sig. wave height	2.64	m
ω_{min}	Min. frequency	0.25	rad s^{-1}
ω_{max}	Max. frequency	3.00	rad s^{-1}
$d\omega$	Frequency increment	0.01	rad s^{-1}

G. *Body dimensions*

Five dimensions define the body in the system presented in Fig. 1. These include water depth h, flap height H_f, distance from the hinge to the seabed c, width w, and thickness p. If the height of the flap is constrained such that the flap always extends from the hinge to the free surface (i.e., $H_f = h\text{-}c$), the thickness is parameterized as function of width ($w/p = constant$), and if the mean water depth is assumed constant, the number of free dimensions can be reduced to two: the flap width and the distance from the hinge to the seabed.

Here, the flap width w ranges from 1/3 of the water depth to the full water depth (the flap is as wide as the water is deep) in increments of 1 m. The distance from the hinge to the seabed c ranges from 0 m to 2/3 of the water depth in increments of 1 m. Though the theoretical model is reliant on a thin-plate assumption, a thickness is defined to obtain reasonable mass moment of inertia and body volume properties. The width-to-thickness ratio is held constant at $w/p = 30$. To parameterize mass, a mass density ρ_m equivalent to half the water density is assigned. For each set of dimensions, the body mass-moment of inertia and linear, combined hydrostatic and gravitational restoring coefficient are calculated using (31) and (32). These dimensions and properties are defined in Table 3.

TABLE 3
DIMENSIONS AND PROPERTIES OF DEMONSTRATION MODEL

Symbol	Name	Value	Unit
h	Water depth	30	m
c	Hinge to seabed	0:1:20:[a]	m
H_f	Flap height	10:1:30	m
w	Flap width	10-30	m
w/p	Flap width-to - thickness ratio	30	m/m
ρ_m	Mass density	500	kg m^{-3}

[a] *start:stepsize:stop*

H. Variation of hydrodynamic coefficients with frequency

Variations in frequency-dependent pitch-added mass, pitch radiation damping, and pitch excitation moment with normalized width (w/H_f) are presented in Fig. 3. Results are shown for a single flap height of $H_f = h/2$. As width is increased, these coefficients increase in magnitude, and peak values shift toward lower frequencies. These trends are consistent with WAMIT results from Kurniawan and Moan [15], who conducted a similar frequency-domain sweep across widths on a bottom-raised OSWEC. Similar trends have been well-documented in studies on bottom-fixed OSWECs [17][18].

I. Parametric study on width and height

Performance characteristics, displayed as a function of the normalized distance to seabed (c/h) and normalized width (w/h), are presented in Fig. 4. The capture width ratio (subfig. a) is representative of the ratio of power absorbed by an ideal PTO during operation in the IWS 2 sea state to the total wave power available in that sea state, obtained using (33)-(40). The surge force at the hinge (subfig. b) and its resulting contribution to the bending moment about the foundation base (subfig. c) are taken as the maximum values in response to a regular design wave at the significant wave height and peak period.

Under the constraints used in the demonstration calculations, the CWR increases dramatically with increasing width and decreases slightly as the distance from the seabed increases. The maximum surge hinge reaction force follows a similar trend. This result is expected; as the OSWEC grows in width or height (recall $H_f = h\text{-}c$), its face occupies a larger portion of the water cross-section, hence increasing the magnitude of the hydrodynamic coefficients and excitation loads. The foundation base bending moment is maximized at the full width and at the largest distance from the seabed. Though the surge hinge reaction force decreases with increasing distance, this change is overcome by the increase in moment arm as the hinge is moved further from the seabed. As both the capture width ratio and hinge surge foundation force are maximized at the same condition (i.e., when w/h is maximized and c/h is minimized, over their observed ranges), a conclusive argument cannot be made as to the optimal dimensions without further constraints. These constraints could include knowledge of the structural limits of the internal hinge support mechanisms (e.g., bearings, shafts, shaft mounts, etc.), as well as the geometry and material limits of the foundation. This trade-off between power absorption and loading on OSWEC designs has been the subject of previous studies [13][14][19]. Contributions from the hydrodynamic loading on the foundation itself, as well as the PTO torque, are not included in this calculation. The effect of these loads on the bending moment may be significant depending on the size and shape of the foundation, as well as the magnitude of PTO damping coefficient.

V. CONCLUSIONS

An understanding of the relationships between key performance characteristics and the parameters in the available design space is fundamental to the design process. Closed-form mathematical models, which benefit from their ease of implementation and fast performance, are well-suited for this task. In this study, the work of Michele *et al.* [1] is extended to model the hydrodynamic characteristics of a bottom-raised OSWEC. Closed-form formulas for pitch-pitch and surge-pitch added inertia and radiation damping are presented. The results are employed to investigate the power production as well as the structural load on the support foundations due to the motion of the OSWEC.

Theoretical values of the hydrodynamic coefficients were validated with numerically obtained results from WAMIT. Overall, the trends are well-captured. Excellent agreement (within 2%) was recorded for added mass, radiation damping, and wave excitation force/torque magnitudes in both pitch-pitch and surge-pitch directions. On the other hand, variations between the analytically and numerically predicted wave-excitation phases are noted at higher frequencies. While the analytical phase angles show convergence toward zero as the frequency increases, the data from WAMIT indicate an offset close to 30 degrees.

Discrepancies in the wave excitation force and torque phase angles could be driven by the thin-plate assumption of the theoretical model, as well as differences in boundary conditions between the theoretical model and WAMIT, the latter of which does not model the presence of a flow-blocking foundation. Investigations into these variations at the high-frequency region will be explored further in a subsequent study.

The model was used in a demonstration study to perform a rapid sweep of design parameter space. Variations in pitch-pitch added mass, radiation damping, and excitation moment were explored as a function of frequency for a range of widths. These trends agreed well with numerical studies presented in the literature. Finally, trends in power performance and measures of the dynamic structural loading from the OSWEC on the foundation were observed over a range of widths and hinge heights. The well-known trade-off between power

absorption and structural loading was highlighted. With further implementation, a designer could use this theoretical model in conjunction with a multi-objective optimization method to quickly narrow free parameters to a near-optimal subset.

APPENDIX

Numerical Accuracy Validation

The analytical model can be validated by evaluating the exciting torque on the structure employing two approaches. The first method employs the surface integral of the scattered potential while the second technique utilizes the Haskind-Hanaoka relation. Using the first approach, the exciting torque was derived in [1] as

$$X_5 = -i\omega\rho f_o \frac{w}{2}\int_0^{2\pi} \phi^S(0,\eta)\sin\eta\, d\eta \tag{43}$$

The result to this expression is presented in Equation (21) with the parameters modified accordingly to account for the bottom-raised effect. On the other hand, using Haskind-Hanaoka relation for 3D floating body, the exciting torque is formulated as (see Chapter 8 in [10] for derivation details).

$$X_5 = -\frac{4}{k}\rho g A \mathcal{A}_R\left(\frac{\pi}{2}\right)\cos\theta \tag{44}$$

$\mathcal{A}_R$ is called the angular variation of the radially spreading wave [10] and having the unit of time.

On the other hand, the general form of asymptotic behavior of the radiation potential in the far field ($\xi \to \infty$) can be written as (Equation 8.6.12 in [10])

$$\sum_{n=0}^{\infty}\phi_n^R \sim \frac{ig\mathcal{A}_R(\eta)}{\omega}\frac{\cosh k(h+z)}{\cosh kh}\sqrt{\frac{2}{\pi kr}}e^{i\left(kr-\frac{\pi}{4}\right)} \tag{45}$$

With $r = \frac{we^{\xi}}{4}$ is the radius expressed in terms of the radial elliptic coordinate ξ [1]. Equating this with equation (17), and using the asymptotic formula of Hankel-Mathieu function of the first kind, $H^{(1)}_{o_{2m+1}}(\xi \to \infty, \tau_n)$, as [11]:

$$H_o(\xi \to \infty, \tau_n) = -\frac{S_{2n+1}}{\sqrt{\tau_n}B_1}\sqrt{\frac{2}{\pi\sqrt{\tau_n}e^{\xi}}}e^{i\left(\sqrt{\tau_n}e^{\xi}-\frac{3\pi}{4}\right)} \tag{46}$$

With $\tau_n = \left(\frac{wk_n}{4}\right)^2$

$$H_o(\xi \to \infty, \tau_n) = -\frac{4S_{2n+1}}{wk_nB_1}\sqrt{\frac{2}{\pi k_n r}}e^{i\left(k_n r-\frac{3\pi}{4}\right)} \tag{47}$$

$\mathcal{A}_R(\eta)$ can then be found as

$$\mathcal{A}_R(\eta) = -\sum_{m=0}^{\infty}\frac{2\omega Z_o f_o\left[se_{2m+1}\left(\frac{\pi}{2},\tau_n\right)\right]^2 se_{2m+1_\eta}(0,\tau_n)}{gk_o Ho_{2m+1_\xi}(0,\tau_n)} \tag{48}$$

Substituting this into equation (44), X_5 can be calculated.

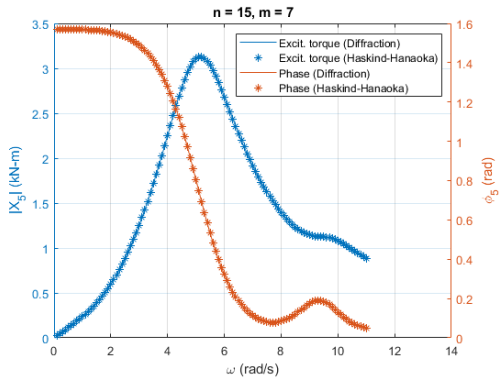

Fig. 5 – Comparison of wave-exciting pitch moment magnitude and phase using 1) Diffraction method and 2) Haskind-Hanaoka relation. The results were obtained with $m = 7$.

Fig. 5 shows the comparison of the wave-excitation pitch moment magnitude and phase using the two approaches with $m = 7$ (the number of orders used in approximating the Mathieu functions). This value of m allows to obtain 1) the difference in the order of $O(10^{-13})$ between the two methods, and 2) the convergences in the wave-exciting pitch and phase values with the maximum differences of 0.27% compared to the results obtained with $m = 6$.

ACKNOWLEDGEMENT

This work was authored in part by the National Renewable Energy Laboratory, operated by Alliance for Sustainable Energy, LLC, for the U.S. Department of Energy (DOE) under Contract No. DE-AC36-08GO28308. Funding provided by the U.S. Department of Energy Office of Energy Efficiency and Renewable Energy Water Power Technologies Office. The views expressed in the article do not necessarily represent the views of the DOE or the U.S. Government. The U.S. Government retains and the publisher, by accepting the article for publication, acknowledges that the U.S. Government retains a nonexclusive, paid-up, irrevocable, worldwide license to publish or reproduce the published form of this work, or allow others to do so, for U.S. Government purposes.

REFERENCES

[1] Dias, Frédéric, Emiliano Renzi, Sarah Gallagher, Dripta Sarkar, Yanji Wei, Thomas Abadie, Cathal Cummins, and Ashkan Rafiee. "Analytical and computational modelling for wave energy systems: the example of oscillating wave surge converters." *Acta Mechanica Sinica* 33, no. 4 (2017): 647-662.

[2] Whittaker, Trevor, David Collier, Matt Folley, Max Osterried, Alan Henry, and Michael Crowley. "The development of Oyster—a shallow water surging wave energy converter." In Proceedings of the 7th European wave and tidal energy conference, pp. 11-14. 2007.

[3] S. Michele, P. Sammarco, and M. d'Errico, "Theory of the synchronous motion of an array of floating flap gates oscillating wave surge converter," *Proc. R. Soc. Math. Phys. Eng. Sci.*, vol. 472, no. 2192, p. 20160174, Aug. 2016, doi: 10.1098/rspa.2016.0174.

[4] I. Noad and R. Porter, "Wave Energy Absorption by Submerged Flap-type Oscillating Wave Surge Converters," p. 8.

[5] E. Renzi and F. Dias, "Resonant behaviour of an oscillating wave energy converter in a channel," *J. Fluid Mech.*, vol. 701, pp. 482–510, Jun. 2012, doi: 10.1017/jfm.2012.194.

[6] E. Renzi and F. Dias, "Hydrodynamics of the oscillating wave surge converter in the open ocean," *Eur. J. Mech. - BFluids*, vol. 41, pp. 1–10, Sep. 2013, doi: 10.1016/j.euromechflu.2013.01.007.

[7] E. Renzi and F. Dias, "Relations for a periodic array of flap-type wave energy converters," *Appl. Ocean Res.*, vol. 39, pp. 31–39, Jan. 2013, doi: 10.1016/j.apor.2012.09.002.

[8] Michele, Simone, Paolo Sammarco, M. d'Errico, Emiliano Renzi, A. Abdolali, G. Bellotti, and F. Dias. "Flap gate farm: From Venice lagoon defense to resonating wave energy production. Part 2: Synchronous response to incident waves in open sea." Applied Ocean Research 52 (2015): 43-61.

[9] P. Schmitt and B. Elsaesser, "On the use of OpenFOAM to model oscillating wave surge converters," *Ocean Eng.*, vol. 108, pp. 98–104, Nov. 2015, doi: 10.1016/j.oceaneng.2015.07.055.

[10] Mei, Chiang C., Michael Stiassnie, and Dick K-P. Yue. *Theory and applications of ocean surface waves: nonlinear aspects*. Vol. 23. World scientific, 2005.

[11] Julio C. GutiÈrrez-Vega, ìFormal analysis of the propagation of invariant optical Öelds in elliptic coordinates,îPh. D. Thesis, INAOE, MÈxico, 2000.
[http://homepages.mty.itesm.mx/jgutierr/]

[12] S. Michele, P. Sammarco, and M. d'Errico, "Weakly nonlinear theory for oscillating wave surge converters in a channel," J. Fluid Mech., vol. 834, pp. 55–91, Jan. 2018, doi: 10.1017/jfm.2017.724.

[13] N. Tom, Y.-H. Yu, and A. Wright, "Balancing the Power-to-Load Ratio for a Novel Variable Geometry Wave Energy Converter with Nonideal Power Take-Off in Regular Waves," p. 11, 2017.

[14] N. M. Tom, Y.-H. Yu, A. D. Wright, and M. Lawson, "Balancing Power Absorption and Fatigue Loads in Irregular Waves for an Oscillating Surge Wave Energy Converter," in *Volume 6: Ocean Space Utilization; Ocean Renewable Energy*, Busan, South Korea, Jun. 2016, p. V006T09A028, doi: 10.1115/OMAE2016-55046.

[15] A. Kurniawan and T. Moan, "Characteristics of a Pitching Wave Absorber with Rotatable flap," *Energy Procedia*, vol. 20, pp. 134–147, 2012, doi: 10.1016/j.egypro.2012.03.015.

[16] F. R. Driscoll *et al.*, "Methodology to Calculate the ACE and HPQ Metrics Used in the Wave Energy Prize," NREL/TP--5000-70592, 1426063, Mar. 2018. doi: 10.2172/1426063.

[17] N. M. Tom, M. J. Lawson, Y. H. Yu, and A. D. Wright, "Development of a nearshore oscillating surge wave energy converter with variable geometry," *Renew. Energy*, vol. 96, pp. 410–424, Oct. 2016, doi: 10.1016/j.renene.2016.04.016.

[18] R. P. F. Gomes, M. F. P. Lopes, J. C. C. Henriques, L. M. C. Gato, and A. F. O. Falcão, "The dynamics and power extraction of bottom-hinged plate wave energy converters in regular and irregular waves," *Ocean Eng.*, vol. 96, pp. 86–99, Mar. 2015, doi: 10.1016/j.oceaneng.2014.12.024.

[19] N. Tom, Y.-H. Yu, A. Wright, and M. Lawson, "Balancing Power Absorption Against Structural Loads With Viscous Drag and Power-Takeoff Efficiency Considerations," *IEEE J. Oceanic Eng.*, vol. 43, no. 4, pp. 1048–1067, Oct. 2018, doi: 10.1109/JOE.2017.2764393.